https://doi.org/10.33472/AFJBS.6.5.2024. 7559-7575

AfricanJournalofBiological Sciences

Reliability and Accuracy of Cone Beam Computed Tomography in Detection and Assessment of Simulated Periodontal Defects: An in-vitro study

Ahmed Aasy[1*], Gehan G. El-Desouky[2], Wael S. Amer[2]

1* Department of Oral radiology, October 6th University, Giza, Egypt

2 Department of Oral and Maxillofacial Radiology, Faculty of Dentistry, Suez Canal University, Ismailia, EGY

* Corresponding author

e-mail: ahmadhusseinaasy@gmail.com

Tel: +201068233328

Article History
Volume 6, Issue 5, 2024
Received: 15 May 2024
Accepted: 22 May 2024
doi:*10.33472/AFJBS.6.5.2024. 7559-7575*

Abstract

Periodontal diseases consist of various conditions that affect the periodontal tissues and their integrity. Diagnosis of periodontal conditions and defects that occur as sequelae of periodontitis, like infra-bony defects, dehiscence, and fenestration, requires thorough clinical and radiographic examinations. With the introduction of 3D imaging, image manipulation and navigation using specialized software were made possible for obtaining high-quality images, leading to better diagnosis. The introduction of CBCT has brought a series of advantages to the field of diagnostic dental imaging over conventional radiographic techniques, including the elimination of distortion and the ability to visualize structures in all planes, in addition to its lower radiation dose, user-friendly software, accuracy, and availability in comparison to CT. Aim: In the present study, the aim was to compare two different resolutions of CBCT in terms of diagnostic performance, accuracy, and reliability in specific circumstances like small periodontal defects and lesions. Materials and methods: a total of 79 periodontal defects, resembling infra-bony defects (IBD), dehiscence, and fenestrations, were created using round burs of different sizes on eight dry human skulls. The linear measurements of each defect were recorded using a digital caliper and were considered the 'gold standard'. The defects were scanned with high- and standard-resolution CBCT. Results: Regarding all defects created, high-resolution CBCT showed no statistically significant difference when compared to the gold standard. High-resolution CBCT showed higher accuracy with a statistically significant difference when compared to standard-

resolution CBCT. In small-sized defects (1-2) standard resolution CBCT showed a statistically significant difference when compared to the gold standard, while in large-sized defects (3-4), standard resolution CBCT showed no statistically significant difference when compared to the gold standard. Conclusions: From the results of this study, it was concluded that high-resolution CBCT is superior to standard-resolution CBCT for the detection of simulated size 1- and 2-mm IBD, fenestration, and dehiscence defects. Close results were also seen regarding the larger-sized simulated defects of 3 and 4 mm.
Keywords: Reliability, Accuracy, CBCT, Cone Beam Computed Tomography, Simulated Periodontal Defects,

Introduction

Periodontitis consists of a wide range of inflammatory conditions that cause periodontal defects and degeneration of the periodontium, with subsequent loss of teeth, facial contour, and aesthetics (Lee et al., 2018).

In periodontitis, infraosseous defects occur when the base of the defect is at an apical location relative to the bone crest. Defects within or inside the bone are termed “intrabony”, while “infra-bony” describe defects “just below the crest of bone” (Goldman and Cohen, 1958).

Periodontitis can result in intrabony defects like dehiscences and fenestration defects and infra-bony defects (IBD) like intrabony pockets (IBPs), IBP occurs when the bottom of the pocket is apical to the level of the adjacent alveolar bone (Weinberg and Eskow, 2000).

Dehiscence is defined as a V-shaped defect located at the alveolar bone margin (ABM) and extending toward the apex. It may be located on the buccal or lingual surfaces of a tooth. The incidence of dehiscences is 7.30% to 27.46%, dehiscences are more frequent in the mandible than in the maxilla (11.55% vs 1.86%) (Leung et al., 2010).

Fenestration, on the other hand, is an isolated area in which the root is denuded of bone and the root surface is only covered by the periosteum and its overlying gingiva with intact marginal bone. The incidence of fenestration ranges between 7.5% and 20%. The percentage is

higher in the maxillary than the mandibular teeth. Moreover, it is higher in the anterior than in the posterior teeth (Nimigean et al., 2009; and Wong et al., 2021).

In periodontitis, alveolar bone loss is considered a dental problem that requires an accurate assessment of the true extension of the borders of the defect for the proper formulation of an effective treatment plan (Anter et al., 2016). Two-dimensional radiographic evaluation (bitewing, periapical, and panoramic radiographs) can play a limited role in establishing and confirming the primary diagnosis regarding damage to the alveolar bone due to inherited drawbacks (Lindhe et al., 2015; Highfield, 2009). The use of CBCT overcame these drawbacks and brought a series of advantages to the field of diagnostic dental imaging over 2D techniques, including the elimination of superimposition and distortion and the ability to visualize structures in all planes (Ludlow et al., 2006; Murali and Bhandary, 2022; Nasim et al., 2018).

The aim of the present study was to compare two different resolutions of CBCT in terms of diagnostic performance, accuracy, and reliability in the assessment of specific small periodontal defects and lesions.

Materials and Methods

Study setting:

The present research was conducted in the Oral and Maxillo-Facial Radiology Department, Faculty of Dentistry, Suez Canal University, on eight dry human skulls of unknown age, sex, or ethnicity, on which periodontal defects were created resembling infra-bony defects, dehiscence, and fenestration, and scanned with high-resolution CBCT and standard-resolution CBCT. Skulls were obtained from the Human Anatomy Department, Faculty of Medicine, Cairo University. The study obtained an ethical approval number of OMP-1-9-2023 (Research Ethics Committee, Sinai University, Faculty of Dentistry).

Inclusion criteria:

The skulls were selected in the present study based on the following eligibility criteria: (1) Adult skulls—partial or full dentition—with no metal fillings or appliances; (2) no pre-existing periodontal defect; and (3) the absence of conditions that may affect the integrity of the alveolar bone.

Creation of the defects:

On the eight skulls, 79 periodontal defects (IBP, dehiscence, and fenestration) were created and distributed in their alveolar processes: 32 in the maxillae and 47 in the mandibles. Twenty-two defects were created in the premolar area, while 57 were created in the molar area (either maxillary or mandibular). The defects were created using a low-speed handpiece and a micro-motor of 800 rpm with round diamond burs of one, two, three, and four millimeters in diameter. Therefore, the dimensions of the created defects were 1mm, 2mm, 3mm, and 4mm for the IBPs, dehiscences, and fenestrations (Pragati and Neelam; 2020; Mark et al., 2021).

The 79 defects were created, resembling different common periodontal conditions. The conditions include that IBPs were created starting from the proximal surface of the tooth at the crest of the alveolar bone, proceeding in an apical direction within the body of the alveolar bone tangent to the root of the involved tooth, creating a total of 31 IBPs (Figure 1.a).

In addition, fenestration was created at the level of the apical part of the root using a round diamond bur at the center of the root on the facial alveolar bone (labial / buccal) and extending circumferentially. Fenestrations were created only on the buccal and labial surfaces of the maxillae and mandibles of the dry skulls, creating a total of 16 fenestration defects (Leung et al., 2010) (Figure 1.b).

Moreover, dehiscence was created on the labial, buccal, lingual, and palatal surfaces of the maxillae and the mandibles of the dry skulls, creating a total of 32 dehiscences. The dehiscence was created starting from the alveolar crest and proceeding in an apical direction, but this time the defects were created in a superficial pattern where the inner wall of the defect was the root of the involved tooth (Caton et al., 2018) (Figure 1.c).

The dimensions of the created defects were measured twice with a digital caliper of 0.1mm accuracy and were repeated by the same operator after two-week intervals. The mean of both readings was assigned as the gold standard (Figure 1.d).

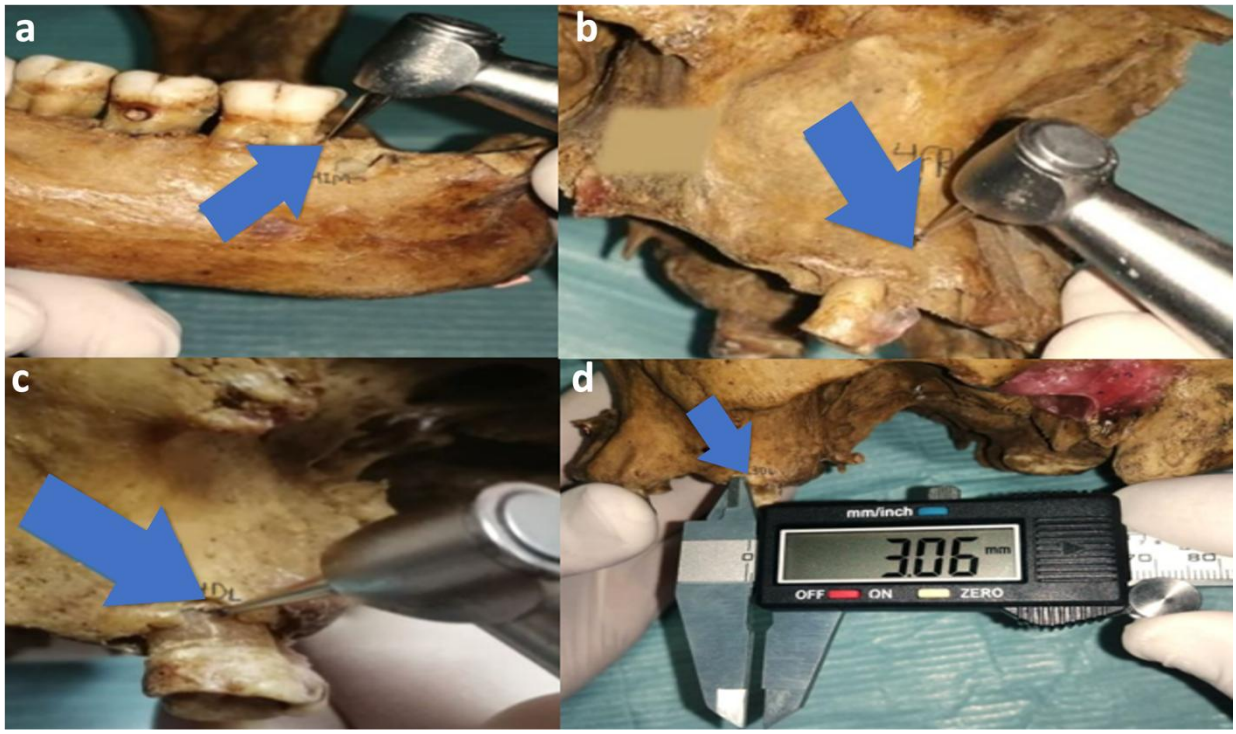

Figure 1: Creating the defects using a slow-speed handpiece and round burs (a). Infra-bony defect on proximal surface (b). Fenestration defect at the apical one-third of the tooth (c). Dehiscence defect at the buccal surface of the alveolar bone crest (d). Measurement of value using the digital caliper.

Ten layers of pink wax, each of 1.5 mm thick (Total thickness of 15mm) were then applied to the facial surface of the skulls, starting from the infraorbital rim to the lower border of the mandible, to simulate the thickness of soft tissue coverage in those areas and to mimic the clinical exposure conditions and attenuation factors for the human head (Richard et al., 2004).

Radiographic examination and assessment:

The CBCT scanner used in the present study was Scanora 3dx (Scanora 3D, Finland, Helsinki TM), KVp: 60-90, mA: 4-10, scan time: 2.4-6, focal spot: 0.5. Detector: flat panel (a-Si.). The skulls were imaged twice, once with high resolution and another time using standard resolution.

For high-resolution CBCT, the scanner was set at XL FOV (80x165-mm), 10 mA, and 90 kV for a single scan of 360˚ rotation and a total scan time of 4 sec, with a voxel size of 0.25 mm and a total exposure dose of 1427 mGycm2. While for standard resolution, the scanner was similarly set at XL FOV (80x165-mm), 10 mA, and 90 kV for a single scan of 360˚ rotation and a total scan time of 2.4 sec, with a voxel size of 0.4mm and a total exposure of 856 mGycm2.

Conclusively, each dry skull was scanned twice using both the high and standard resolutions, with voxel sizes of 0.25-mm and 0.4- mm, respectively.

The detection of defects and measurement of their dimensions from both scanning resolutions was performed on a personal computer using On-Demand software using ruler tool for linear measurements.

For intra-bony defects, measurements were made on coronal cuts starting at the crest of the alveolar bone until the deepest point of the pocket (Figure 2).

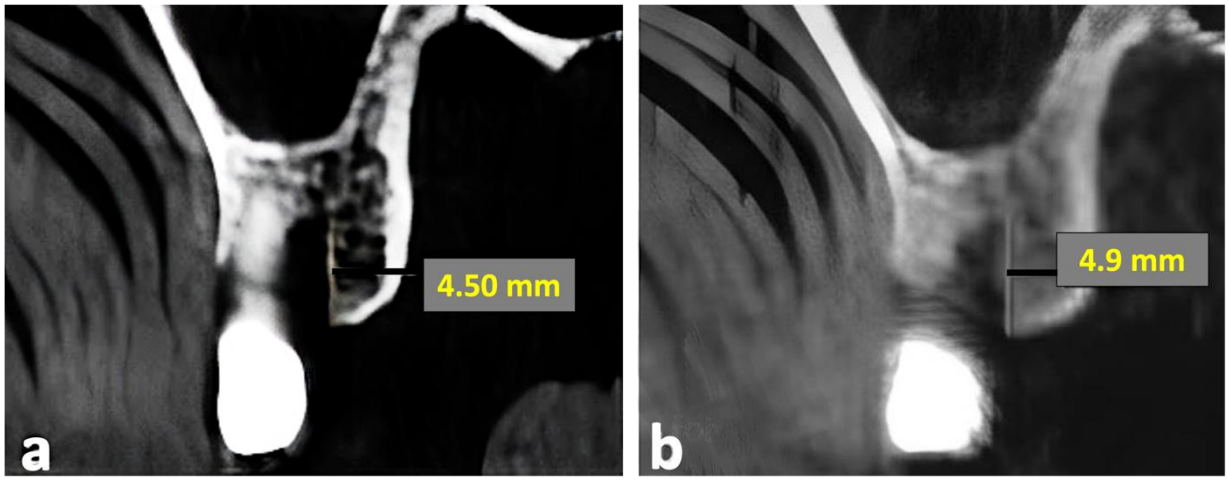

Figure 2: Measurements of an infra-bony defect (a). High-resolution CBCT (b). Standard resolution CBCT on coronal views.

For dehiscence, measurements were made on a volume rendered (VR) view between the edges of the defect tangent to the apical root surface (Figure 3).

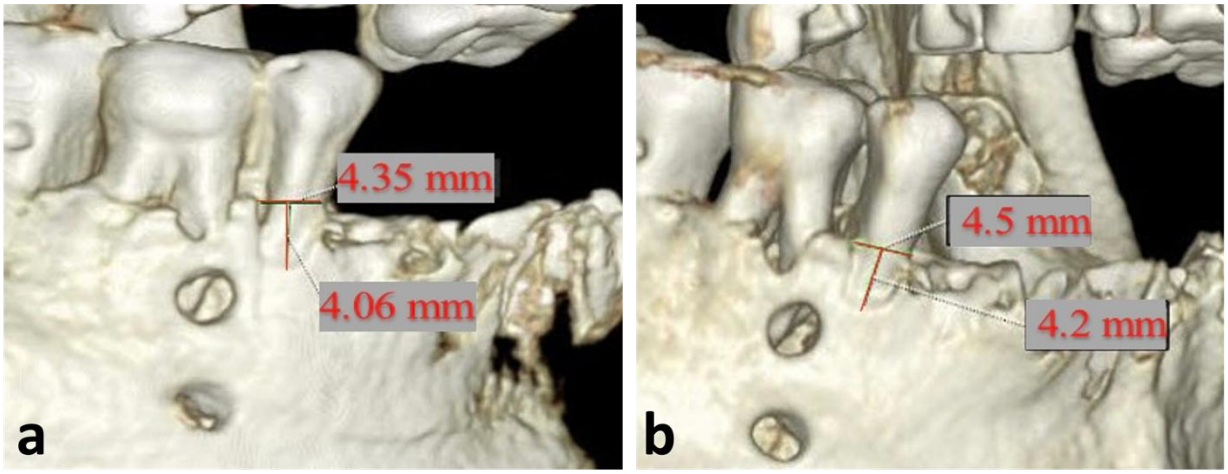

Figure 3: Measurements of the created dehiscence defect (a). High-resolution CBCT (b). Standard resolution CBCT on 3D volume rendering.

Fenestration measurements were also made on a VR view to measure the diameter of the fully made circular defect tangent to the apical root surface (Figure 4).

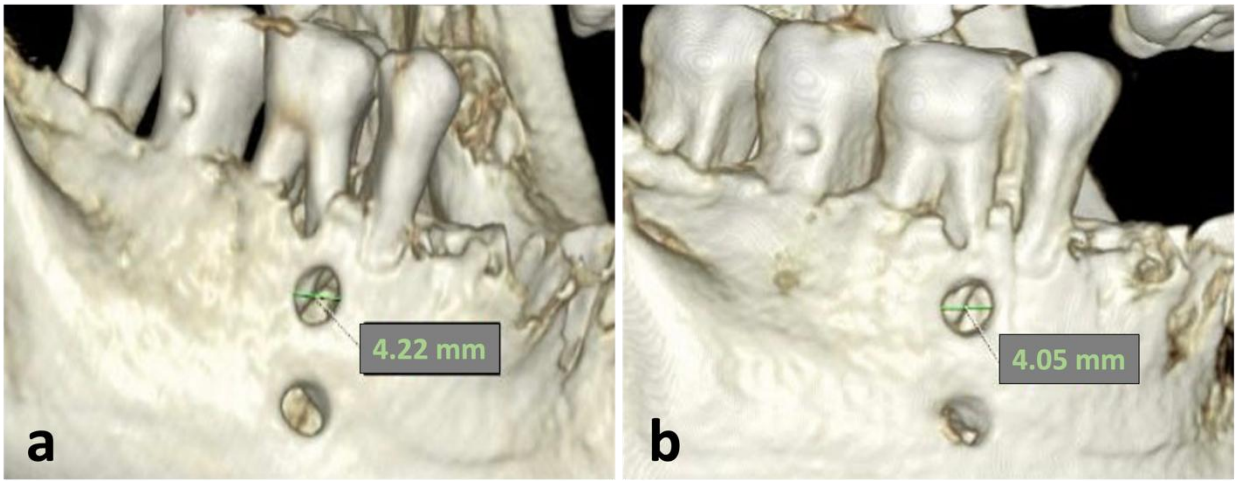

Figure 4: Measurements of the created fenestration defect (a). High-resolution CBCT (b). Standard resolution CBCT on 3D volume rendering.

Measurements for all defects from both resolutions were recorded for comparison with the gold standard. Measurements from standard and high-resolution CBCT scans were made once and repeated two weeks later by the same observer for intra-observer reliability analysis.

Statistical Analysis

In the present study, the radiographic measurements of created defects (IBP, dehiscence and fenestration) obtained from high and standard CBCT scans were compared to the actual clinical measures obtained using a digital caliper. The collected numerical data was summarized using means and standard deviations. The recorded data was then tabulated for statistical analysis.

In the current study, Cronbach's alpha and interclass coefficient (ICC) analyses were used to measure internal consistency between the intra-observer records and determine how closely they were related.

To state whether the recorded data was significant or non-significant, ANOVA test was used. Since it allows a comparison of more than two groups at the same time to determine whether a relationship exists between them or not. Comparisons between linear actual measurements (gold standard) and radiographic measurements were made using the independent Duncan's Multiple Range Test (DMRT). All p-values were two-sided (estimated values may be more than or less than the reference value). P-values≤0.05 were considered significant.

Results

Reliability analysis performed for assessment of intra-observer reliability showed very close intra-observer agreement varying from 0.922 to 1.00 for both readings obtained for the gold standard physical measurements, standard resolution, and high resolution CBCT scans using Cronbach's alpha and interclass coefficient (ICC) analysis.

Table (1) represents the mean and standard deviation (SD) values and comparison between gold standard, high and standard CBCT resolutions for the infra-bony pockets (1, 2, 3 and 4 mm).

For sizes 1mm and 2mm IBP, the mean value of high-resolution CBCT showed a statistically non-significant difference ($p>0.05$) when compared to the gold standard, while the mean value of standard-resolution CBCT showed a statistically significant difference ($p<0.05$) when compared to the gold standard. The difference between high versus standard CBCT resolutions was statistically significant ($p=0.007$* for 1mm) ($p<0.001$** for 2mm).

For sizes 3mm and 4mm IBP, the mean value of both high-resolution and standard-resolution CBCT showed a statistically non-significant difference (p>0.05) when each was compared to the mean value of the gold standard. The difference between high and standard CBCT resolutions in relation to the gold standard was statistically non-significant (p>0.05).

Table 1: Comparison between gold standard, high-resolution CBCT, and standard-resolution CBCT images regarding the created IBPs.

Defect size	IBD (Mean±SD)				
	Gold standard	High resolution CBCT	Standard resolution CBCT	ANOVA rep. measures F	*p*-value
1mm	1.13 ± 0.06^{b}	1.14 ± 0.03^{b}	1.33 ± 0.25^{a}	4.97	0.007^{*}
2mm	2.08 ± 0.14^{b}	2.07 ± 0.21^{b}	2.48 ± 0.18^{a}	15.87	$<0.001^{**}$
3mm	3.23 ± 0.24^{a}	3.24 ± 0.23^{a}	3.36 ± 0.23^{a}	0.95	0.432^{ns}
4mm	4.14 ± 0.13^{a}	4.13 ± 0.13^{a}	4.21 ± 0.15^{a}	1.03	0.395^{ns}

*, **: significant at p<0.05, 0.01, 0.001; ns: non-significant at p>0.05. Means followed by different letters (^{a}/^{b}) in the same row (horizontally) are significantly different according to DMRTs at 0.05 level.

Means followed by different letters (a/b) in the same row (horizontally) are significantly different according to DMRTs at the 0.05 level.

Table (2) presents the mean and standard deviation and results of the comparison between the gold standard, high and standard CBCT resolutions for the dehiscence defects (1, 2, 3 and 4 mm).

For 1mm and 2mm dehiscence, the mean value of high-resolution CBCT showed a statistically non-significant difference (p>0.05) when compared to the mean value of the gold standard, while the mean value of standard-resolution CBCT showed a statistically significant difference (p<0.05) when compared to the mean value of the gold standard. The differences between gold standard and high resolution CBCT versus low resolution CBCT were statistically significant (p=0.005 for 1mm dehiscence and p<0.001** for 2mm dehiscence).

For size 3mm and 4mm dehiscence, the mean values for high resolution and standard resolution CBCT showed a statistically non-significant difference (p>0.05) when compared to the mean value of the gold standard.

Table 2: Comparison between gold standard, high resolution CBCT, and standard resolution CBCT regarding the created dehiscence defects.

Defect size	Dehiscence (Mean±SD)			ANOVA rep. measures	
	Gold standard	High resolution CBCT	Standard resolution CBCT	F	*p*-value
1mm	1.19 ± 0.11^{b}	1.19 ± 0.10^{b}	1.48 ± 0.17^{a}	16.47	0.005^{*}
2mm	2.14 ± 0.16^{b}	2.12 ± 0.16^{b}	2.51 ± 0.12^{a}	17.86	$<0.001^{**}$
3mm	3.15 ± 0.18^{b}	3.24 ± 0.23^{b}	3.55 ± 0.22^{a}	8.15	0.002^{*}
4mm	4.14 ± 0.14^{a}	4.14 ± 0.15^{a}	4.22 ± 0.16^{a}	0.84	$>0.05^{ns}$

*, ** significant at p<0.05, 0.01, 0.001; ns, non-significant at p>0.05. Means followed by different letters (^{a}/^{b}) in the same row (horizontally) are significantly different according to DMRTs at 0.05 level.

Table (3) presents the mean and standard deviation (SD) values of the study data and comparison between the gold standard and high- and standard-resolution CBCT for the fenestration defects (1, 2, 3 and 4 mm).

Similarly, for size 1mm, 2mm, and 3mm fenestration, the mean value for high-resolution CBCT showed a statistically non-significant difference (p>0.05) when compared to the mean value of the gold standard, while the mean value for standard-resolution CBCT showed a statistically significant difference (p<0.05) when compared to the gold standard. The differences between gold standard and high resolution CBCT in comparison to the standard resolution CBCT were statistically significant (p<0.001**) for 1mm and 2mm and (p=0.030* for 3mm dehiscence).

For size 4mm fenestration, the mean values for high- and standard-resolution CBCT showed a statistically non-significant difference (p>0.05) when compared to mean value of the gold standard.

Table 3: Comparison between the gold standard, high-resolution CBCT, and standard-resolution CBCT regarding the created fenestration defects.

Defect size	Fenestration (Mean±SD)			ANOVA rep. measures	
	Gold standard	High resolution CBCT	Standard resolution CBCT	F	*p*-value
1mm	1.03 ± 0.05^{b}	1.08 ± 0.07^{b}	1.48 ± 0.16^{a}	43.97	$<0.001^{**}$

2mm	2.07 ± 0.08 [b]	2.07 ± 0.04 [b]	2.31 ± 0.13 [a]	19.39	<0.001**
3mm	3.17 ± 0.14 [b]	3.18 ± 0.09 [b]	3.33 ± 0.13 [a]	4.18	0.030*
4mm	4.04 ± 0.12 [a]	4.02 ± 0.08 [a]	4.33 ± 0.37 [a]	4.78	0.019*

*, **: significant at p<0.05, 0.01, 0.001; ns: non-significant at p>0.05. Means followed by different letters ([a]/[b]) in the same row (horizontally) are significantly different according to DMRTs at 0.05 level.

Discussion

Alveolar bone destruction in periodontitis can result in IBP that can get deeper than 6 mm, and other defects like dehiscence and fenestration, which can cause tooth loss, subsequently affect the quality of periodontal patients' lives. Early detection of alveolar bone loss in periodontitis is critical for maintaining a healthy periodontium, the proper treatment outcome, and the prognosis (Kim et al., 2004; Herrera et al., 2018).

The use of CBCT in periodontology began with the evaluation and prognosis of treatment outcomes for periodontitis. Afterwards, more studies were performed to study the sensitivity of the CBCT in the assessment of undetected periodontal bone pathology such as interproximal defects, furcation involvement, diagnosis of dehiscence and fenestration and post-surgical results of regenerative periodontal therapy. CBCT has been shown to have a sensitivity of 80-100% in the detection and classification of induced bony defects (Mohan et al., 2011).

However, the use of CBCT in the field of periodontology is still rather limited because of the higher radiation dose involved when compared to conventional radiographs. Several studies were conducted on the selection of the optimum resolution needed for the detection of periodontal problems, keeping in mind the goal of radiation dose reduction (Mohan et al., 2011). Hence, the aim of the present study was to evaluate the accuracy and reliability of CBCT in the detection and assessment of induced periodontal problems with different sizes using CBCT with standard and high resolutions for optimizing its clinical application in the detection of bony lesions in periodontally affected patients.

The current study was conducted on dry adult skulls to ensure that the alveolar process is fully developed, with enough mineral content and with no pre-existing periodontal condition

and/or defects for convenient creation of the defects, proper examination and optimum visualization on radiographs (Zhao et al., 2015).

Following the guidelines of Zhang et al.(2015) careful examination of the skulls was performed to ensure that there were no present boney abnormalities that would change the density of the alveolar bone and subsequently affect the creation of the defects in a way that mimics their pathologically occurring counterparts.

The dried skulls were selected without any metallic fillings, appliances, or metallic prosthetic parts to avoid any possible effect on the accuracy of measurements from CBCT images that may be the result of metallic artifacts such as scatter and beam hardening. This was in accordance with Scarfe and Angelopoulos (2018) who stated that the image data set can sometimes be utterly useless for diagnostic purposes when streak artifacts that arise from metallic objects obscure anatomical structures in the affected slices, interfering with the clear visibility of structures in the vicinity of, or in between, metallic objects, and hence could affect the accuracy of the linear measurements.

To avoid inaccuracies in the size and integrity of the margins of the defects, in the current study we used a low-speed motor of 800 rpm for better control while creating the defects and diamond round burs of sequential sizes of 1mm, 2mm, 3mm and 4mm to create periodontal defects equivalent to the burs sizes for standardized size of the defects and to produce sharper margins for better measurement recording and reading (Bagis et al., 2018).

To simulate true beam attenuation in clinical situations, a total thickness of 14.5mm thickness of pink wax sheets for each 1cm of muscles was applied to the dry skulls as muscle and soft tissue replacement to simulate soft tissue of the facial muscles as recommended by Richard et al. (2004), Schropp et al. (2003) and Caldas et al. (2010).

In our study, we used a fixed FOV (XL 80x165-mm) with two different imaging protocols of voxel sizes of 0.2mm for high-resolution and 0.4mm for standard resolution. To evaluate the more accurate resolution and voxel size for optimization and application in clinical situations where precise and accurate evaluation is needed for periodontal defects.

Reliability analysis was performed for all measurements obtained in our study to assess the accuracy of the readings obtained by the observer at different time intervals. The results for

intra-observer agreement in the current study showed firm agreement between the two observations, which indicated the reliability and standardization of the method of assessment used in the study.

Regarding the IBP, the results of high-resolution CBCT showed markedly superior accuracy in assessing the smallest lesions (1mm) in comparison to that of standard-resolution CBCT in relation to the gold standard, where the standard-resolution CBCT was unable to detect the presence of these defects. Regarding the smaller lesions (2mm), high-resolution CBCT again showed increased accuracy in terms of detection and evaluation, superior to standard CBCT scan assessing these defects, Again, the standard CBCT was unable to detect small-sized defects.

Concerning the medium-sized defects (3mm), a slightly higher accuracy for high-resolution CBCT compared to that of the standard-resolution CBCT was shown. Finally, regarding the large defects (4mm), high-resolution CBCT still showed superior accuracy for assessment of the IBP compared to the standard-resolution CBCT (in relation to the gold standard), however, the difference was statistically insignificant. Moreover, with medium and large defects, the detectability of the defects was not of paramount difficulty in contrast to the standard CBCT. A finding revealed that the accuracy and detectability of the created defects increased with an increase in the size of the defect for the two protocols.

These findings were consistent with those of Kolsuz et al. (2015), and his colleagues, who concluded that high-resolution CBCT should be requested for small-sized defects; otherwise, a standard-resolution CBCT is sufficient for routine examination and detection of large-sized defects (4mm).

Our findings were also in line with Samaneh et al. (2016) and his colleagues, who concluded that high-resolution CBCT was superior in assessment of Grade I furcation involvements, three-wall defects, dehiscence, and fenestrations.

In the current study, regarding dehiscence and fenestration, high-resolution CBCT showed superior accuracy over standard-resolution CBCT in terms of accurate assessment and evaluation of the simulated defects, especially for fenestration.

Icen et al. (2020) conducted another study on 12 dry skulls with a maxilla and mandible. Artificial defects were created related to teeth separately using burs randomly on the dry skulls to

compare the diagnostic accuracy of CBCT of different voxel sizes to detect and assess periodontal defects. They concluded that smaller voxel sizes and smaller CBCT FOV have the highest sensitivity and diagnostic accuracy for detecting various periodontal defects (dehiscence, fenestration, furcation involvement) among the scanner modalities examined. The findings from their study were consistent with those of our study.

The limitation in our study was the use of burs to create artificial defects instead of acid etching. Acid etching creates defects with borders that emulate naturally occurring periodontal defects.

Conclusion

CBCT is an important tool when diagnosing alveolar bone loss in chronic periodontitis. However, due to its relatively high radiation dosage, CBCT should be implemented for diagnosis following safe guidelines. High resolution CBCT is superior to standard resolution CBCT for spotting the simulated infra-bony, fenestration and dehiscence defects. Fenestrations are better detected than dehiscence on both CBCT scanning protocols. After through periodontal clinical examination, if small sized periodontal defects are expected, high resolution CBCT (with smallest available FOV) should be requested for accurate diagnosis of the present periodontal defect.

References

Anter E, Zayet MK, El-Dessouky SH (2016): Accuracy and precision of cone beam computed tomography in periodontal defects measurement (systematic review). J Indian Soc Periodontol. 2016, 20:235-43. 10.4103/0972-124X.176389

Bagis N, Eren H, Bilecenoğlu B, et al. (2018) Comparison of the burr and chemically induced periodontal defects using different field-of-view sizes and voxel resolutions. Oral Surgery, Oral Medicine, Oral Pathology, and Oral Radiology. 2018, 125(3):260-267. 10.1016/j.oooo.2017.11.010

Caldas MDP, Ramos-Perez FMDM, Almeida SMD, et al.(2010): Comparative evaluation among different materials to replace soft tissue in oral radiology studies. Journal of Applied Oral Science. 2010, 18:264-267. 10.1590/s1678-77572010000300012.

Caton JG, Armitage G, Berglundh, et al. (2018) A new classification scheme for periodontal and peri- implant diseases and conditions-Introduction and key changes from the 1999 classification. Journal of periodontology. 2018, 20:S1-S8. 10.1111/jcpe.12935

Goldman, HM, & Cohen, DW (1958) The Infrabony Pocket: Classification and Treatment. Journal of Periodontology. 1958, 29:291. 10.1902/jop.1958.29.4.272

Herrera D, Retamal- Valdes B, Alonso B & Feres M (2018) Acute periodontal lesions (periodontal abscesses and necrotizing periodontal diseases) and endo- periodontal lesions. Journal of clinical periodontology. 2018, 89(1):S85-S102. 10.1002/JPER.16-0642

Highfield J. (2009) Diagnosis and classification of periodontal disease. Aust Dent. 2009, 54:1:S11-26. 10.1111/j.1834-7819.2009.01140.x

Icen M, Orhan K, Şeker Ç, et al. (2020) Comparison of CBCT with different voxel sizes and intraoral scanner for detection of periodontal defects: An in vitro study. Dentomaxillofacial Radiology. 2020, 49(5):20190197. 10.1259/dmfr.20190197

Kim CS, Choi SH, Chai JK, et al. (2004) Periodontal repair in surgically created intrabony defects in dogs: influence of the number of bone walls on healing response. 2004. 2004, 75(2):229-235. 10.1902/jop.2004.75.2.229

Kolsuz ME, Bagis N, Orhan K, et al.(2015) Comparison of the influence of FOV sizes and different voxel resolutions for the assessment of periodontal defects. Dentomaxillofacial Radiology. 2015, 44(7):20150070. 10.1259/dmfr.20150070

Lee JH, Kim DH, Jeong SN, et al. (2018) Diagnosis and prediction of periodontally compromised teeth using a deep learning-based convolutional neural network algorithm. Journal of periodontal & implant science. 2018, 48:114-123. 10.5051/jpis.2018.48.2.114

Leung CC, Palomo L, Griffith R, et al. (2010) Accuracy and reliability of cone-beam computed tomography for measuring alveolar bone height and detecting bony dehiscences and fenestrations. Am J Orthod Dentofacial Orthop. 2010, 137:109-19. 10.1016/j.ajodo.2009.07.013

Lindhe J, Lang NP, Karring T (2015) Clinical periodontology and implant dentistry. Lindhe J, Karring T, Araújo M, editors. The anatomy of periodontal tissues, Singapore:

Blackwell Publishing Ltd pp. 3-8. Lang NP, and Lindhe J (ed): Blackwell Publishing Ltd , Singapore; 2015. 6th:1480.

Ludlow JB, Davies-Ludlow LE, Brooks SL, et al. (2006) Dosimetry of 3 CBCT devices for oral and maxillofacial radiology. CB Mercuray, NewTom 3G and i-CAT. Dentomaxillofacial Radiology. 2006, 35(4):219-226. 10.1259/dmfr/14340323

Mark R, Mohan R, Gundappa M, et al. (2021) Comparative evaluation of periodontal osseous defects using direct digital radiography and cone-beam computed tomography. Journal of Pharmacy & Bioallied Sciences. 2021, 13(1):S306-S311. 10.4103/jpbs.JPBS_804_20

Mohan R, Singh A & Gundappa M (2011) Three-dimensional imaging in periodontal diagnosis-Utilization of cone beam computed tomography. Journal of Indian Society of Periodontology. 2011, 15(1):11-7. 10.4103/0972-124X.82256

Murali AC, & Bhandary R (2022) Cone-Beam Computed Tomography in Periodontal Diagnosis and Treatment Planning. Journal of Health. 2022, 47(1):25-37. 10.3290/j.qi.a34724

Nasim A, Mohan RPS, Nagaraju K, et al. (2018) Application of Cone Beam Computed Tomography Gray Scale Values in the Diagnosis of Cysts and Tumors. J Indian Acad Oral Med Radiol 30: 4-9. 2018, 30(1):4-9. 10.4103/jiaomr.jiaomr_4_18

Nimigean VR, Nimigean V, Bencze MA, et al. (2009) bone dehiscences and fenestrations:an anatomical study and review. Romanian Journal of Morphology and Embryology. 2009, 50:391-397.

Pragati D. and Neelam M. (2020): Periodontal diseases- A brief review. International Journal of Oral Health Dentistry. 6.177-187. 10.18231/j.ijohd.2020.038

Richard YH, Nojima K, Adams WP, et al. (2004) Analysis of Facial Skin Thickness: Defining the Relative Thickness Index. American society of plastic surgeons. 2004, 115(6):1769-73. 10.1097/01.prs.0000161682.63535.9b

Samaneh Bayat, Ahmad Reza Talaeipour, Fatemeh Sarlati (2023): Detection of simulated periodontal defects using cone-beam CT and digital intraoral radiography. Dentomaxillac Radiology. 2016, 45(6):20160030. 10.1259/dmfr.20160030.

Scarfe W C & Angelopoulos C (2018) Maxillofacial Cone beam computed tomography: principles, techniques, and clinical applications. Springer. Scarfe W C & Angelopoulos C (ed): Springer international Publishing AG, Switzerland; 2018. 10.1007/978-3-319-62061-9

Schropp L, Wenzel A, Kostopoulos L, and Karring T (2003) Bone healing and soft tissue contour changes following single-tooth extraction: a clinical and radiographic 12-month prospective study. International Journal of Periodontics and Restorative Dentistry, vol. 2003, 23(4):313-323.

Weinberg, MA, & Eskow, RN (2000) Osseous defects: proper terminology revisited. Journal of Periodontology. 2000, 71:1928. 10.1902/jop.2000.71.12.1928

Wong J, Lee A, Zhang C (2020) Diagnosis and Management of Apical Fenestrations Associated with Endodontic Diseases: A Literature Review. Eur Endod J. Apr. 2021, 6:25-33. 10.14744/eej.2020.51422

Zhang X, Li Y, Ge Z, et al. (2020) The dimension and morphology of alveolar bone at maxillary anterior teeth in periodontitis: a retrospective analysis—using CBCT. International Journal of Oral Science. 2020, 12(1):1-9. 10.1038/s41368-019-0071-0

Zhao H, Li C, Lin L, et al. (2015) Assessment of alveolar bone status in middle aged Chinese (40-59 Years) with chronic periodontitis—using CBCT. PLoS One. 2015, 10(10):e0139553. 10.1371/journal.pone.0139553